RSC Advances

ROYAL SOCIETY OF CHEMISTRY

www.rsc.org/advances

One-pot Hydrothermal Synthesis of Carbonaceous Nanocomposites for Efficient Decontamination of Copper

Tian Longlong[a,b‡], Liu Dan[a,c‡], Huang Lingxin[a], Cao Shiwei[d], Qi Wei[a], Lin Jing[a], Wu qiang[a], Li Zhan[e*], Wu Wangsuo[a*]

[a] Lanzhou University, Lanzhou, Gansu, China, 730000; [b] Soochow University, Suzhou, Jiangsu, China,215000; [c] Wuhan University, Wuhan, Hubei, China, 430000; [d] Institute of Modern Physics, Chinese Academy of Sciences, Lanzhou, 730000, China; [e] Lanzhou Institute of Chemistry Physics, Chinese Academic of Science，Lanzhou, Gansu, China, 730000.

[*]Corresponding author: Li Zhan, Email: lizhancg@licp.cas.cn; Wu Wangsuo, Email: wuws@lzu.edu.zn

[‡]These authors contributed equally to this work

Abstract

Environmental pollution associated to heavy metal ions has always been a serious environment problem. As so far, carbonaceous adsorbents are still the promising candidates for the decontamination of these ions, but limited by either cost or adsorption capacity. Here, carbonaceous nanocomposites containing numerous surface acidic groups were easily synthesized *via* one-pot hydrothermal carbonization of glucose in the presence of acrylic acid and little graphene oxide, and characterized in detail. Then batch adsorption of Cu(II) on the carbonaceous nanocomposites from aqueous solution showed that materials exhibited excellent adsorption affinity for Cu(II) and the maximum adsorption capacity was as high as 146.1 mg/g at pH 5 and *T* = 298 K, which was much higher than any previous reports. The effect of degree of functionality on adsorption behaviors, as well as the effect of pH, ionic strength, complex anion, temperature, and the presence of natural organic compounds (humic acid and fulvic acid) and organic pollutant (ionic liquid), were studied systematically

to understand the adsorption mechanism. Besides, X-ray photoelectron spectroscopy was further used to confirm surface complexion reaction played an important role in the adsorption process. This work would provide cheap nanocomposites which could be candidate materials for efficient decontamination of copper ions.

Introduction

The pollution of heavy metal ions in industrial wastewater has attracted global attention due to its adverse effects on the environment and human health[1, 2]. Copper, an abundant and natural occurring element present in municipal wastewaters[3], is one of the most widespread and common heavy metal contaminants in the environment[4]. Many methods have been investigated to remove Cu(II) from wastewaters such as chemical precipitation, adsorption, ion exchange, membrane separation, reverse osmosis, electrolysis froth flotation and solvent extraction[5, 6]. Among these methods, adsorption has increasingly received more attention as it's simple and cost effective. Up to now, various adsorbents have been used to remove Cu(II), such as soil, clay mineral[7] and resins [3, 8, 9]. However, all things considered, these materials suffer from either high cost or low adsorption capacity, which limit their value for further study.

Carbonaceous materials are promising adsorbents for they are facile and environment friendly[10]. But standard methods for the manufacture of activated carbons usually require very harsh conditions and have several drawbacks[11]. What's worse, the adsorption capacity of activated carbon needs to be further enhanced[12]. Graphene oxide[13] and carbon nanotubes[14] have showed high adsorption capacities due to their large specific surface areas and numerous surface functional groups[15-17], while their application still remains at theory stage[18].

Here, a new type of carbonaceous nanocomposites was synthetized easily *via* one-step aqueous hydrothermal carbonization route using cheap glucose in the presence of acrylic acid and few graphene oxide. The weight ratio of glucose to graphene oxide was fixed at 24 to lower cost and acquire large specific surface area[19]. And acrylic acid added in the reaction could offer abundant functional groups and adsorption sites. The prepared materials, containing rich acidic groups, not only were inexpensive and easy to get, but also exhibited very excellent adsorption affinity and

high maximum adsorption capacity for Cu(II) adsorption. In order to assess the adsorption capacity of the as-prepared materials and understand the adsorption mechanism, batch experiments, including the effect of pH, ionic strength, complex anion and temperature, were studied and combined with the X-ray photoelectron spectroscopy [20]. Considering the presence of many natural organic compounds in the real environment, both humic acid and fulvic acid were valuated[21]. What's more, the presence of 1-Butyl-3-methylimidazolium chloride ([Bmim][Cl]) was also studied, for it was the most used water soluble ionic liquid[22] and also a potential contaminant[23].

Experiment

Materials preparation

Firstly, graphene oxide was prepared by the improved Hummers method[24, 25]. To obtain materials with a high degree of functionality, acrylic acid monomer was added to the reaction mixture of glucose (3.6 g) and graphene oxide (0.15 g) with different amount: 0, 3.6, 7.2 and 10.8 mL (mole ratio of acrylic acid to glucose were 0, 2.5, 5 and 7.5). Then deionized water was added to reach a total volume of 70 mL. And the final mixture was sealed into the Teflon inlet in an autoclave, which was hydrothermally treated at 198 ℃ for 16 h. Then, the materials were washed several times by deionized water and vacuum-dried overnight at 50 ^{o}C. Final products obtained were ultrasonically dispersed in deionized water as stock suspension (1 mg/mL).

Characterization

The prepared materials were collected and characterized by element content analysis (EC), scanning electron microscopy (SEM), transmission electron microscopy (TEM), X-ray photoelectron spectroscopy (XPS), Raman spectroscopy, Fourier transform infrared (FTIR) spectroscopy, powder X-ray diffraction (PXRD) and potentiometric titration. EC was examined with a Vario EL (ELEMENTAR). SEM was examined using with MIRA 3 XMU (Tecan). TEM was examined using a Tecnai-G2-F30 Field Emission Transmission Electron Microscope (FEI Corporation). Raman spectra from 500 to 4000 cm^{-1} were collected on an inVia-Reflex Raman

scope using a 632.8 nm He-Ne laser (Renishaw). FTIR spectra were recorded from 400 to 4000 cm^{-1} on a NEXUS 6705-DX 170SX spectrometer (Nicolet Instrument Corporation). XPS spectra was examined using an ESCALAB 250Xi (Thermo Fisher Scientific). PXRD was pattern was scanned from 5 ° to 60 ° on X'Pert PRO X-ray diffractometer (Panalytical).The potentiometric acid–base titrations were conducted under argon using a DL50 Automatic Titrator (Mettler Toledo) in NaCl as background electrolyte.

Adsorption Experiments

Batch adsorption experiments were carried out at 200 rpm equivalent shaking rate in 10 mL polyethylene test tubes for 24 h. The stock suspension of adsorbents and the stock solutions of Cu(II) were added in polyethylene test tubes to achieve the desired concentrations of different components (solid-to-liquid ratio was fixed at 0.2 g/L). In most experiments, solution pH was adjusted to 2-10 as measured with a pH-meter (pHS-3C, Shanghai). For cases where pH was adjusted, a 0.1 mol/L NaOH or HCl solution was used to change the initial pH value. A 5 mol/L NaCl ($NaNO_3$ or $NaClO_4$) background electrolyte solution was used to adjust ionic strength. After each adsorption equilibrium, mixtures were centrifuged and the concentration of Cu(II) in supernatant was determined by an Atomic Absorption Spectroscopy (AAS, Perkin-Elmer). Adsorption amount was calculated according to the difference of Cu(II) concentrations before and after adsorption. Adsorption isotherms were run by taking different concentrations of Cu(II) at fixed temperature (298 K) and pH (5.0). At each condition, adsorption experiments were performed in triplicate and then took the average.

Adsorption kinetics fitting model

The pseudo-second-order model[26, 27] general form was:

$$\frac{t}{Q_t} = \frac{1}{kQ_e^{\,2}} + \frac{1}{Q_e}t$$

Where t (h) is the contact time, Qt (mg/g) is the adsorption amount at time t, Qe (mol/g) is the adsorption amount at the equilibrium time, and k [g/(mg·h)] is the pseudo-second-order rate constant.

Adsorption isotherm fitting model

The General Langmuir Freundlich model[28, 29] was employed to fit the adsorption data. Its general form was:

$$Q_e = Q_m \frac{(kC_e)^{\alpha}}{1 + (kC_e)^{\alpha}}$$

Where Q_e (mg/g) is the amount of Cu(II) adsorbed on the adsorbent; Q_m (mg/g) is the maximum amount of Cu(II) adsorbed per unit mass of the adsorbent; C_e (mg/L) is the adsorbate concentration at equilibrium; k (L/mg) is the adsorption affinity coefficient; and α is an indicator of isotherm nonlinearity related to the heterogeneity of sorption sites.

Results and Discussion

Characterization results

It has been reported that three-dimensional graphene-based porous materials at the bulk scale were synthesized via hydrothermal carbonization of glucose and graphene oxide[19]. The reported materials showed large specific surface areas, but lacked surface functional groups for adsorption of metal ions. So we added acrylic acid as a comonomer to the reaction mixture of glucose and graphene oxide to provide more surface functional groups. For instance, GA0, GA1, GA2 and GA3 respectively represented 0, 3.6, 7.2 and 10.8 mL acrylic acid used in the reaction. Fig. 1 showed the morphologies images of materials. Compared to the smooth surface of GA0 (Fig. 1a), large amount of carbon nanodots (~ 2.8 nm, Supplementary Information Fig. S1) were found to be deposited on the surface of GA1, GA2 and GA3 (Fig. 1c, b and d). And the SEM images (Fig. 1e and f) of the materials confirmed that the surface of materials became rough after adding acrylic acid. The morphological characterization results proved that adding acrylic acid successfully enhanced surface functional groups.

Element content analysis (Table 1) revealed that the oxygen content increased with the increasing of acrylic acid volume in the reaction. Comparing with that of precursors, an oxygen content of 38.6% seemed to be very high for final product.

FTIR spectra of the products were recorded (Fig. 2a), and the following functional groups were identified in all samples: O–H stretching vibrations (3431 cm^{-1}), C=O stretching vibration (1705 cm^{-1}), C=C from sp^2 carbon (1627 cm^{-1}), C–O vibrations (1406 cm^{-1}), and O-H bending vibration (1203 cm^{-1})[25]. XPS (Fig. S4) and Raman (Fig. 2b) were used to further analyze the carbon hybridization and oxygen-containing functional group state. The characteristic peaks of D-band (1360 cm^{-1}) and G-band (1601 cm^{-1})[24] were clear in Raman spectra. And the results that the I_D/I_G of GA0, GA1, GA2 and GA3 gradually reduced indicated that the sp^2 carbon content increased with the increasing of acrylic acid volume in the reaction, because the carbon atoms in acrylic acid molecule were sp^2 hybridization. The powder X-ray diffraction (Fig. 2c) confirmed the board (002) peak of carbon.

Potentiometric titration were performed under argon atmosphere to characterize the surface charge densities (ΔQ^H, mol/g) and the total concentration of surface acidic groups per solid weight (H_s, mmol/g) of materials[30]. ΔQ^H was determined by subtracting the titration curve of the background electrolyte solution (blank) from that of material suspension. In general, a suspension of material in 50 mL 0.1 mol/L NaCl solution was titrated with a standard NaOH solution (0.05 mol/L) up to pH~10 at room temperature. Fig. 2d showed the results that pH_{PZC} (pH of point of zero charge) depended strongly on oxygen content.

$$(C_a - C_b)_{susp} = [H^+] - [OH^-] + \Delta Q_{solid} + \Delta Q_{blank}$$

$$(C_a - C_b)_{blank} = [H^+] - [OH^-] + \Delta Q_{blank}$$

$$\Delta Q^H = V/m[(C_a - C_b)_{susp} - (C_a - C_b)_{blank}]$$

Where C_a and C_b (mol/L) were the concentrations of acid and base added, respectively; ΔQ_{blank} (mol/L) represented consumption or release of H^+ by side reactions; ΔQ_{solid} (mol/L) and ΔQ^H (mol/g) represented the proton excess of the material in different units, respectively; *V (L)* was the volume of aqueous solution and *m (g)* was the mass of material.

H_s calculated from the two equivalence points on the Gran plot (V_{eb1} and V_{eb2}, Supplementary Information S2 and Table S1) is defined by the following equation:

$$H_s = (V_{eb2} — V_{eb1})C_b/m_s$$

The H_s calculated from the titration curves was listed in Table 1. It was clear that the higher oxygen content, the higher H_s value, while the relationship was non-linear. These characterization results indicated that carbonaceous nanocomposites with different degree of functionality were successfully synthesized (detailed data were summarized in Table 1). Then GA1 was chosen to systematically study the adsorption mechanism.

Kinetics

Fig. 3a showed the adsorption kinetics of Cu(II) on GA1. The adsorption amount increased quickly in the first 1 h, and then slowed down until the adsorption process reached equilibrium, which indicated that the adsorption mechanism was mainly chemical adsorption or surface complexation rather than physical sorption[3]. After simulating several adsorption kinetics models, the pseudo-second-order model was found to be the most suitable (fitting parameter in Table S2) with the correlation coefficient (R^2) of 0.998. Although the adsorption process was fast, the shaking time in the following batch experiments were selected as 24 h to achieve complete equilibrium.

Effect of pH

The pH of the solution influences the surface chemical properties of material and the species of metal ions[31]. So it is important to study the effect of pH on the adsorption behaviors. Fig. 4a showed the adsorption of Cu(II) on GA1 as a function of pH. The sharp increase of adsorption percentage over pH 4 was attributed to the deprotonating of the surface acidic groups which had strong affinity for the positively charged Cu(II) species. According to Cu(II) speciation distribution as a function of pH values (Fig. 4b), Cu(II) began to form precipitation at pH 6 if no Cu(II) was adsorbed, while most Cu(II) were adsorbed by GA1 before pH 6, which proved that the adsorption of Cu(II) was not due to the surface precipitation of $Cu(OH)_{2(s)}$[21]. In order to completely eliminate the influence of Cu(II) precipitation, the adsorption isotherms of Cu(II) on the materials were investigated at pH 5.0.

Effect of ionic strength and anion

The ionic strength and anion are important factors to study the adsorption

mechanism, so the effect of NaCl, $NaNO_3$ and $NaClO_4$ concentration on the adsorption percentage of Cu(II) on GA1 were showed in Fig. 5a. The adsorption was inhibited gradually by NaCl due to strong coordination of Cl^- reducing the actual concentration of Cu(II); while the adsorption was promoted by $NaNO_3$ and $NaClO_4$, suggesting that the oxideacid anion took part in surface complexation. Comparing the adsorption isotherms of Cu(II) on GA1 in the presence of 0.1 mol/L NaCl, $NaNO_3$ or $NaClO_4$ (Fig. 5b, fitting parameters in Table S3), the similar results were observed. The results suggested that the materials were favorable for wastewater containing oxideacid anion.

Effect of temperature

As we all know, temperature is also a key factor to effect on ion absorption. Fig. 6 showed the adsorption isotherms of Cu(II) on GA1 at 298, 313 and 328 K (fitting parameters in Table S4). The temperature showed slightly positive influence on the adsorption behaviors, which indicated that the adsorption of Cu(II) on the GA1 an endothermic process. Some researchers reported that Cu(II) ions had to be denuded of their hydration sheaths to some extent, and this dehydration process needs energy[3, 32]. The materials showed stable adsorption behaviors against temperature.

Effect of the presence of organic compounds

In the natural environment, there were many coexistent organic compounds. So the effect of the presence of humic acid, fulvic acid and [Bmim][Cl] were studied, and the results were shown in Fig. 7 (fitting parameters in Table S5). The results showed that the presence of humic acid and fulvic acid greatly promoted the adsorption capacity, while, on the contrary, the presence of [Bmim][Cl] slightly inhibited the adsorption behaviors. Those organic compounds were easy to be adsorbed by the materials through π-π interaction. And the negatively charged humic acid and fulvic acid[21] were coordinated with the Cu(II), forming Cu-O bond, and also further negatively charged the materials, which significantly improved the adsorption capacity of positively charged Cu(II). However, although the adsorbed $[Bmim]^+$ could form strong Cu-N bond which promoted the adsorption behaviors, the positively charged $[Bmim]^+$ changed the surface charge properties of materials and inhibited further adsorption of

positively charged Cu(II). The results clearly indicated that the numerous natural organic compounds would promote the decontamination process.

Effect of degree of functionality

Four kinds of materials with different degrees of functionality were prepared. The adsorption isotherms of Cu(II) on GA0, GA1, GA2 and GA3 at pH 5, 0.1 mol/L NaCl and T = 298K were shown in Fig. 8. The maximum adsorption amounts (Q_m) of GA0, GA1, GA2 and GA3 were 10.2, 97.2, 122.6 and 146.1 mg/g, respectively. And it seemed to be clear that the higher degree of functionality, the higher adsorption capacity. Modeling the relationship between Q_m and oxygen content or H_s (Fig. 9 and Fig. S5) showed that the Q_m was linearly dependent on H_s (R^2=0.99995). The results indicated that the adsorption behavior was related to the surface acidic groups, not the oxygen content, because some inner oxygen atoms at the hydrothermal carbon layer couldn't adsorb Cu(II). And previous reports also claimed that the adsorption of metal ions on a series of carbons was found to be related to the type and concentration of surface functional groups[33].

To further evaluate our result, XPS studies of GA1 before and after Cu(II) adsorption were conducted. The XPS results (Fig. 10) that relative content of C-O-C/C-OH was reduced, that of C=O/COO increased, and the binding energy (B.E.) shifted after adsorption suggested that oxygen atoms were the main adsorption sites and the Cu^{2+}-O coordinate bonds were formed in adsorption process[5]. And the Cu2p XPS also clearly manifested that Cu(II) was adsorbed on the surface of the material.

Comparing to adsorption capacities of other adsorbents (Table 3), such as modified activated carbon[12], graphene oxide[15] and pecan nutshell[34], adsorption capacity of carbonaceous nanocomposites in this work was as high as 146.1 mg/g, which was the highest.

Competitive adsorption

The competitive adsorption of multi-metal ions on the materials was studied for exploring its potentiality in practical application. The initial solution was prepared with 0.8 mmol/L in each of Cu(II), Sr(II), Zn(II), Mg(II), Ca(II), Cd(II), K(I) and Na(I). After adsorption to carbonaceous nanocomposites, concentrations in

supernatant were determined using ICP-AES, and adsorption percentages were showed in Fig. 11. Adsorptions of Cu(II), Sr(II), and Zn(II) on the materials were higher than that of other five ions, and the adsorption affinity (~48%) of materials to Cu(II) was the strongest as compared with Sr(II) (~26%) and Zn(II) (~14%), which meant that carbonaceous nanocomposites had high potentiality for selectively removing Cu(II).

Conclusion

Carbonaceous nanocomposites with a high degree of functionality were synthesized *via* one-pot hydrothermal carbonization of cheap glucose in the presence of acrylic acid and little graphene oxide. The materials exhibited excellent adsorption affinity for Cu(II) and the maximum adsorption capacity was as high as 146.1 mg/g, which was much higher than any previous reports and linearly dependent on surface acidic groups. The adsorption kinetics showed the adsorption behavior was fast and well fitted with the pseudo-second-order kinetic model. And, more remarkably, the presence of oxideacid anion and natural organic compounds could promote the adsorption behaviors. A schematic diagram elucidating the whole process was illustrated in Fig. 12. Overall, the cheap carbonaceous nanocomposites in this work exhibited high potential for efficient decontamination of copper ions.

Acknowledgements

This project is supported by National Science Foundation of China J1210001, 21327801 and 21405165. The authors thank Professor AFM Rahman and Doctor Zhang Rui for modification of the manuscript.

Reference:

1. J. Duruibe, M. Ogwuegbu and J. Egwurugwu, *Int J Phys Sci*, 2007, 2, 112-118.
2. L. Järup, *British medical bulletin*, 2003, 68, 167-182.
3. X. Wu, D. Zhao and S. Yang, *Desalination*, 2011, 269, 84-91.
4. C. Yuwei and W. Jianlong, *Chemical Engineering Journal*, 2011, 168, 286-292.
5. A. Z. M. Badruddoza, A. S. H. Tay, P. Y. Tan, K. Hidajat and M. S. Uddin, *Journal of Hazardous Materials*, 2011, 185, 1177-1186.
6. F. Fu and Q. Wang, *Journal of Environmental Management*, 2011, 92, 407-418.
7. R. Zhang, C. Chen, J. Li and X. Wang, *Applied Surface Science*, 2015, 349, 129–137.
8. C.-Y. Kuo, *Desalination*, 2009, 249, 781-785.
9. J. He, Y. Lu and G. Luo, *Chemical Engineering Journal*, 2014, 244, 202-208.

10. X. Guo, C. Wang, M. Chen, J. Wang and J. Zheng, *Journal of Power Sources*, 2012, 214, 107-112.
11. R. Demir-Cakan, N. Baccile, M. Antonietti and M.-M. Titirici, *Chemistry of Materials*, 2009, 21, 484-490.
12. L. Monser and N. Adhoum, *Separation & Purification Technology*, 2002, 26, 137-146.
13. R. K. Upadhyay, N. Soin and S. S. Roy, *RSC Advances*, 2014, 4, 3823-3851.
14. J. Wang, Z. Li, S. Li, W. Qi, P. Liu, F. Liu, Y. Ye, L. Wu, L. Wang and W. Wu, *Plos One*, 2013, 8, 1016-1020.
15. X. Ren, J. Li, X. Tan and X. Wang, *Dalton Transactions*, 2013, 42, 5266-5274.
16. G. Huang, W. Wang, X. Mi, W. Xie, Y. Liu and J. Gao, *Carbon*, 2012, 50, 4856-4864.
17. M. Yusuf, F. M. Elfghi, S. A. Zaidi, E. C. Abdullah and M. A. Khan, *RSC Advances*, 2015, 5, 50392-50420.
18. G. Zhao, T. Wen, X. Yang, S. Yang, J. Liao, J. Hu, D. Shao and X. Wang, *Dalton Transactions*, 2012, 41, 6182-6188.
19. L. Zhang, F. Zhang, X. Yang, G. Long, Y. Wu, T. Zhang, K. Leng, Y. Huang, Y. Ma and A. Yu, *Scientific reports*, 2013, 3.
20. G. Sheng, Y. Li, X. Yang, X. Ren, S. Yang, J. Hu and X. Wang, *RSC Advances*, 2012, 2, 12400-12407.
21. X. Tan, M. Fang, J. Li, Y. Lu and X. Wang, *Journal of hazardous materials*, 2009, 168, 458-465.
22. D. J. Gorman-Lewis and J. B. Fein, *Environmental science & technology*, 2004, 38, 2491-2495.
23. B. Jastorff, K. Mölter, P. Behrend, U. Bottin-Weber, J. Filser, A. Heimers, B. Ondruschka, J. Ranke, M. Schaefer and H. Schröder, *Green Chemistry*, 2005, 7, 362-372.
24. D. C. Marcano, D. V. Kosynkin, J. M. Berlin, A. Sinitskii, Z. Sun, A. Slesarev, L. B. Alemany, W. Lu and J. M. Tour, *ACS nano*, 2010, 4, 4806-4814.
25. T. Longlong, Z. Xin, Q. Wei, L. Dan, J. Qiang, L. Jin, Y. Yuanlv, L. Zhan and W. Wangsuo, *RSC Advances*, 2014, 4, 58536-58545.
26. L. Wang, C. Cheng, S. Tapas, J. Lei, M. Matsuoka, J. Zhang and F. Zhang, *Journal of Materials Chemistry A*, 2015, 3, 13357-13364.
27. S. W. Zhang, J. X. Li, T. Wen, J. Z. Xu and X. K. Wang, *Rsc Advances*, 2013, 3, 2754-2764.
28. M. N. Carvalho, C. A. M. De Abreu, M. Benachour, D. C. S. Sales, O. S. Bara17Na and M. A. D. Motta Sobrinho, *Adsorption Science & Technology*, 2012, 30, 691-699.
29. G. P. Jeppu and T. P. Clement, *Journal of Contaminant Hydrology*, 2012, 129-130, 46-53.
30. Q. H. Fan, P. Li, W. S. Wu, D. Q. Pan, K. F. Ding, Y. Lu, T. Yu and J. Xu, *Science China Chemistry*, 2011, 54, 1138-1147.
31. A. Schierz and H. Z01nker, *Environmental Pollution*, 2009, 157, 1088-1094.
32. M. Wang, H. Jiang and Z. C. Wang, *Journal of Thermal Analysis & Calorimetry*, 2006, 85, 751-754.
33. B. Xiao and K. M. Thomas, *Langmuir*, 2005, 21, 3892-3902.
34. J. C. P. Vaghetti, E. C. Lima, B. Royer, B. M. da Cunha, N. F. Cardoso, J. L. Brasil and S. L. P. Dias, *Journal of Hazardous Materials*, 2009, 162, 270-280.

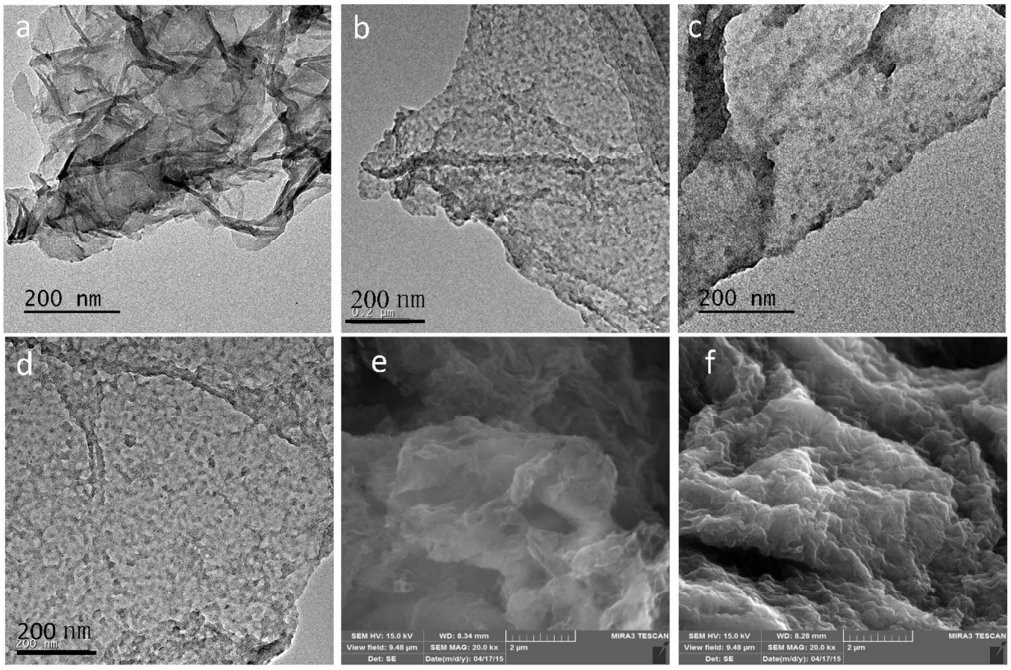

Fig. 1 TEM images of GA0 (a), GA1 (b), GA2 (c) and GA3 (d); SEM images of GA0 (e) and GA1 (f).

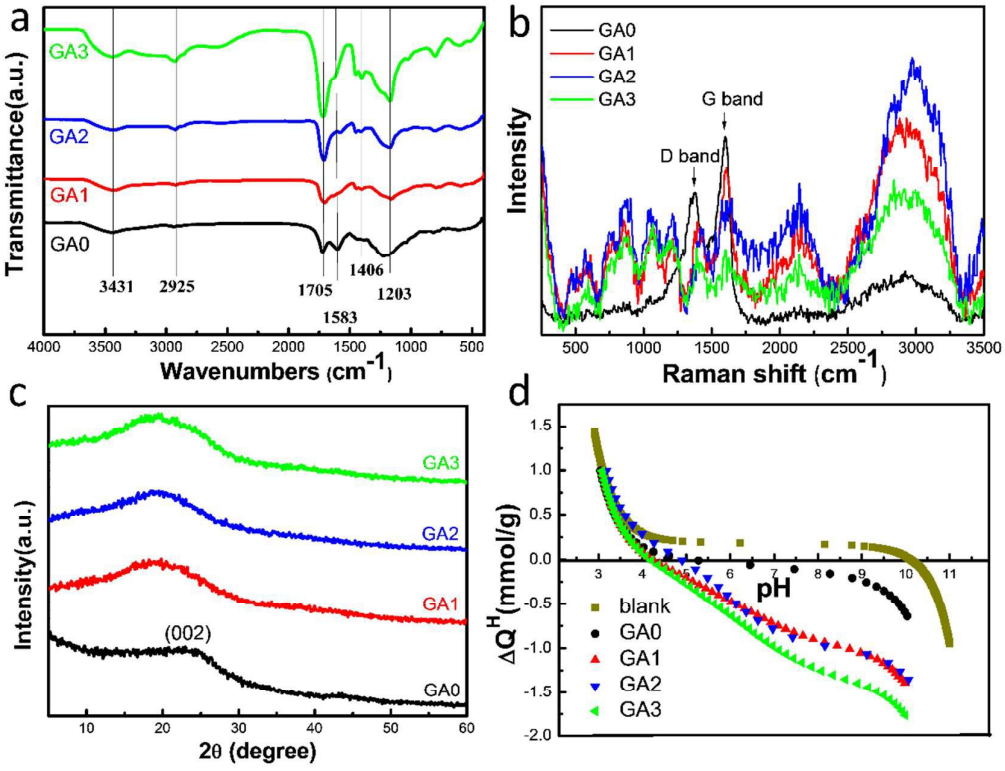

Fig. 2 FTIR (a), Raman spectra (b), XRD (c) and surface charge densities (ΔQ^H) (d) of GA0, GA1, GA2 and GA3.

Table 1 selected properties of the materials

Material	Element Content				I_D/I_G	O1s/C1s	H_s(mmol/g)
	C (%)	O (%)	H (%)	O/C			
GA0	68.15	27.67	4.18	0.41	1.49	0.31	1.48
GA1	63.48	32.34	4.18	0.51	0.56	0.54	5.37
GA2	59.77	35.19	5.03	0.59	0.20	0.74	6.54
GA3	55.97	38.62	5.41	0.69	0.17	0.76	7.57

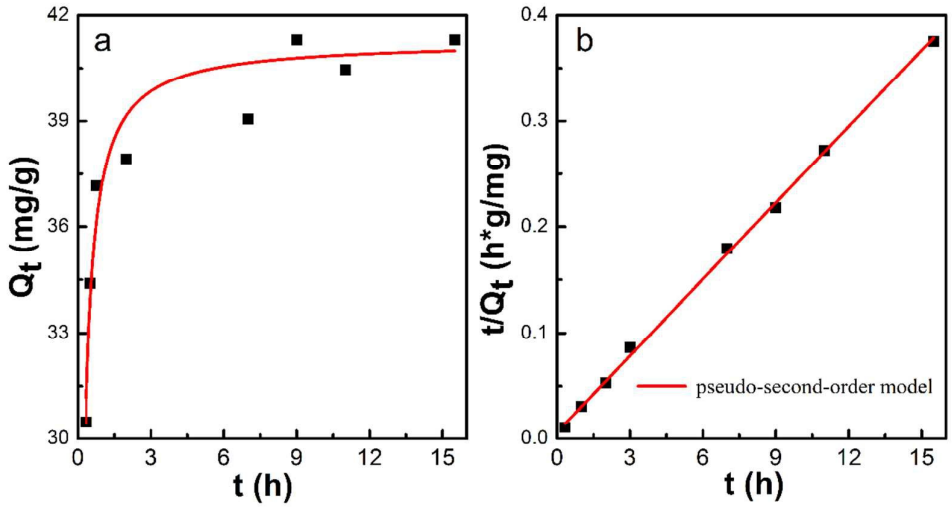

Fig. 3 Adsorption of Cu(II) on GA1 as a function of contact time. (a) Plot of Q_t vs. t for Cu(II) adsorption on GA1. (b) Plot of t/Q_t vs. t for the pseudo-second-order model. T=298 K, pH=5, $C_{Cu(II)}$initial=0.2 mmol/L and I_{NaCl} =0.1 mol/L.

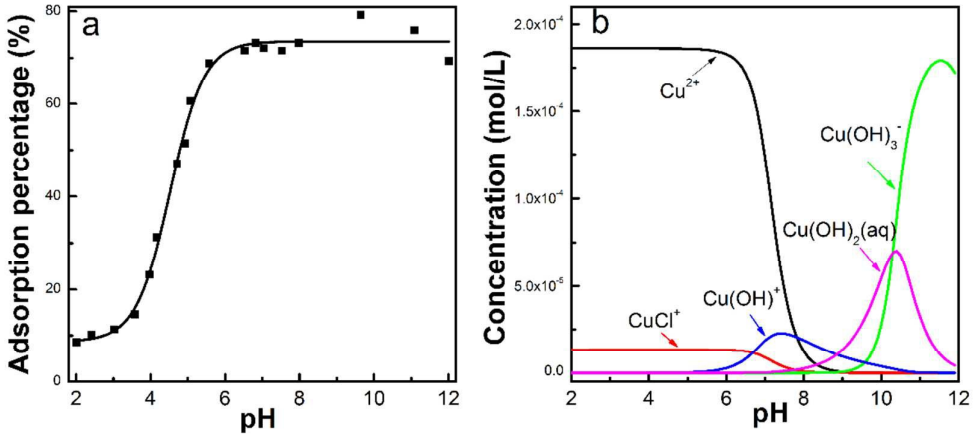

Fig. 4 Adsorption of Cu(II) on GA1 as a function of pH (a), T=298 K, $C_{Cu(II)}$initial=0.2 mmol/L and I_{NaCl} =0.1 mol/L. Concentration of Cu(II) species as a function of pH values (b), T=298 K $C_{Cu(II)}$ =0.2 mmol/L and I_{NaCl} =0.1 mol/L.

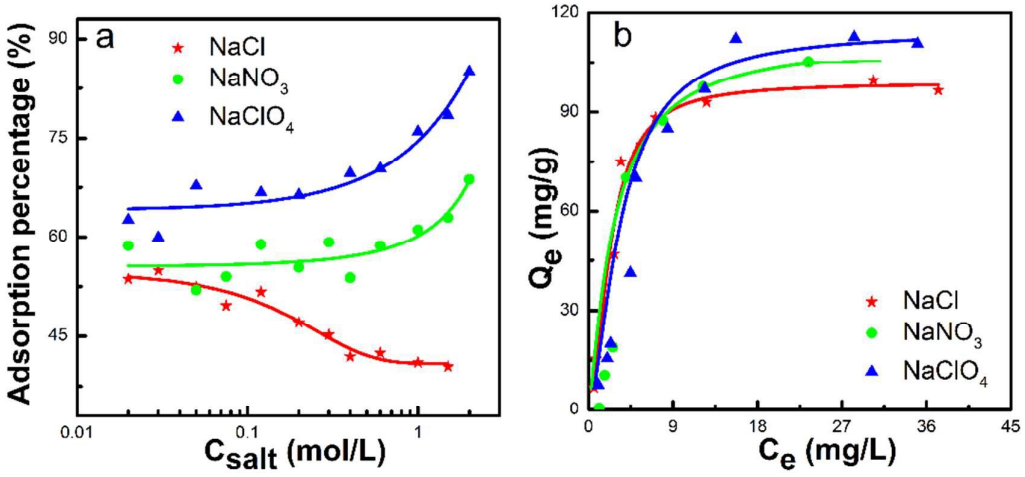

Fig. 5 The effect of NaCl, $NaNO_3$ and $NaClO_4$ concentration on the adsorption percentage of Cu(II) on GA1 at pH=5 and T=298 K (a). Adsorption isotherms of Cu(II) on GA1 in 0.1 mol/L NaCl, $NaNO_3$ and $NaClO_4$, pH=5 and T=298 K (b).

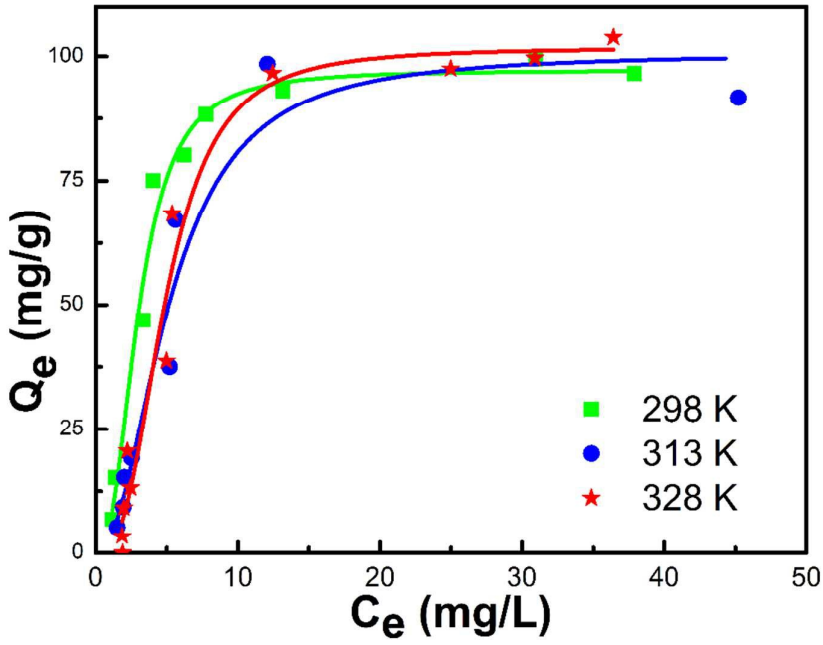

Fig. 6 Adsorption isotherms of Cu(II) on GA1 at pH=5, I_{NaCl}=0.1 mol/L, T=298, 313 and 328 K.

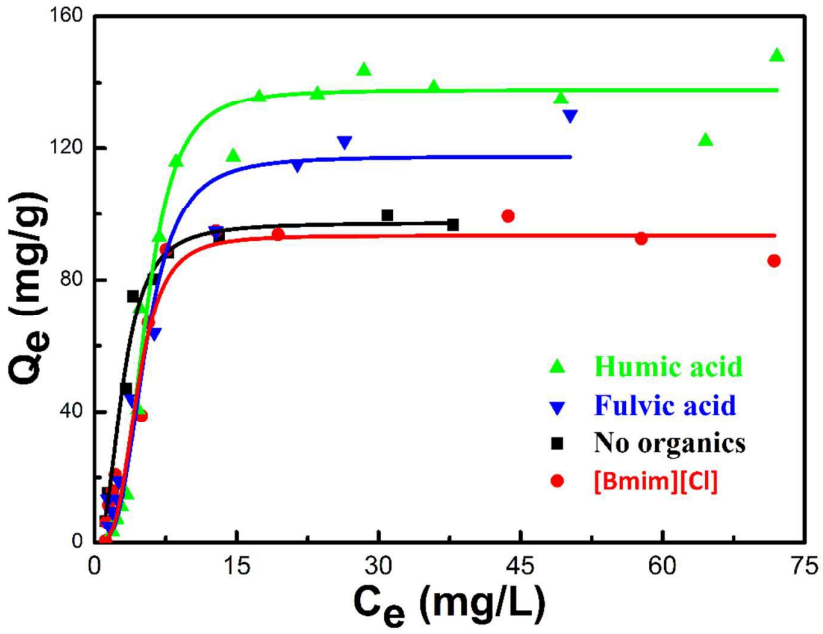

Fig. 7 Adsorption isotherms of Cu(II) on GA1 in the presence of 20 mg/L humic acid, fulic acid and [Bmim][Cl] at pH=5, T=298 K and I_{NaCl}=0.1 mol/L.

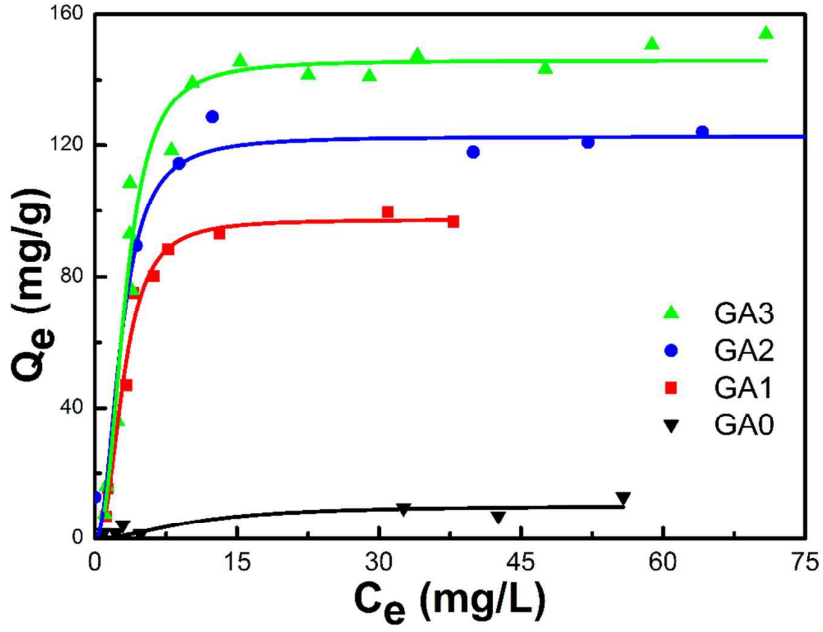

Fig. 8 Adsorption isotherms of Cu(II) on GA0, GA1, GA2 and GA3 at pH=5, T=298 K and I_{NaCl}=0.1 mol/L.

Table 2 The fitting parameters for General Langmuir Freundlich model of Cu(II) adsorption isotherms

Material	Q_m (mg/g)	k	α	R^2
GA0	10.2	0.096	1.85	0.73
GA1	97.2	0.332	2.47	0.98
GA2	122.6	0.358	2.24	0.97
GA3	146.1	0.314	2.46	0.96

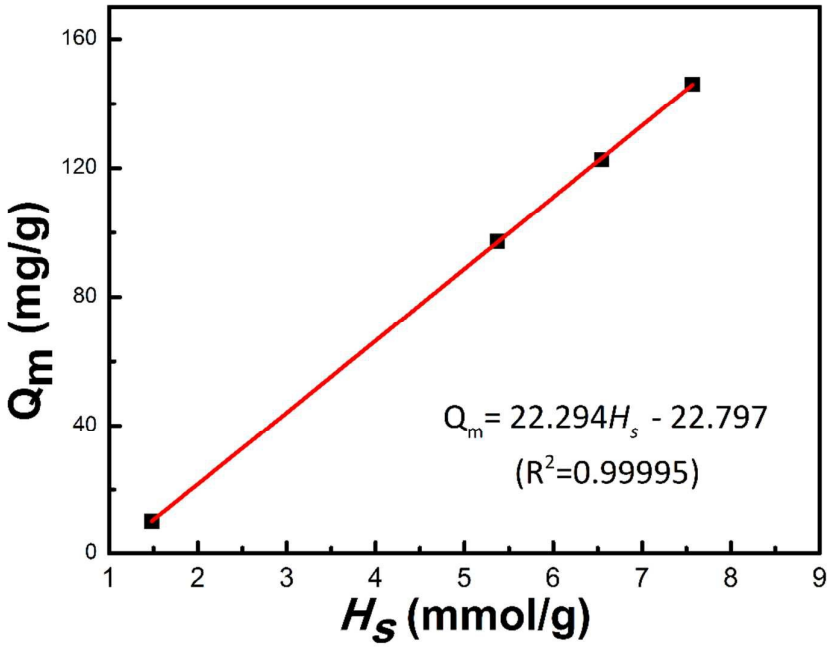

Fig. 9 Relationship between Q_m and H_s.

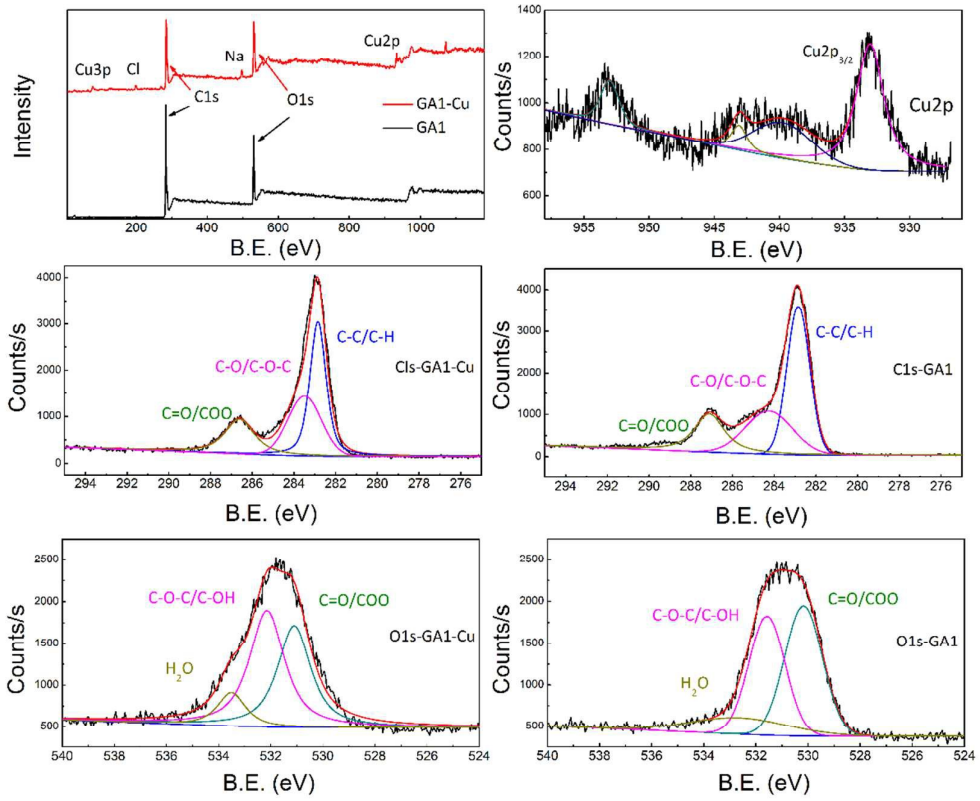

Fig. 10 XPS of GA1 before adsorption (GA1) and after adsorption (GA1-Cu).

Table 3 Comparison of the Cu(II) adsorption capacity of different adsorbents

Adsorbents	Experiment Condition	Q_m(mg/g)	Reference
Graphene Oxide Aerogel	pH= 6.3, T=298K	19.7	[16]
Oxidized Multi-Walled CNTs	pH= 4, T=298K	29.7	[14]
Modified Activated Carbon	pH=5, T=298K	38	[11]
H_2SO_4/$KMnO_4$-Modified CNTs	pH= 6, T=300K	38.6	[8]
CMCD-MNPs	pH= 6, T=298K	47.2	[5]
Graphene Oxide	pH= 5, T=308K	74.9	[15]
Pecan Nutshell	pH= 5.5, T=298K	91.2	[34]
Carbonaceous Nanocomposites	pH= 5, T=298K	**146.1**	**This Work**

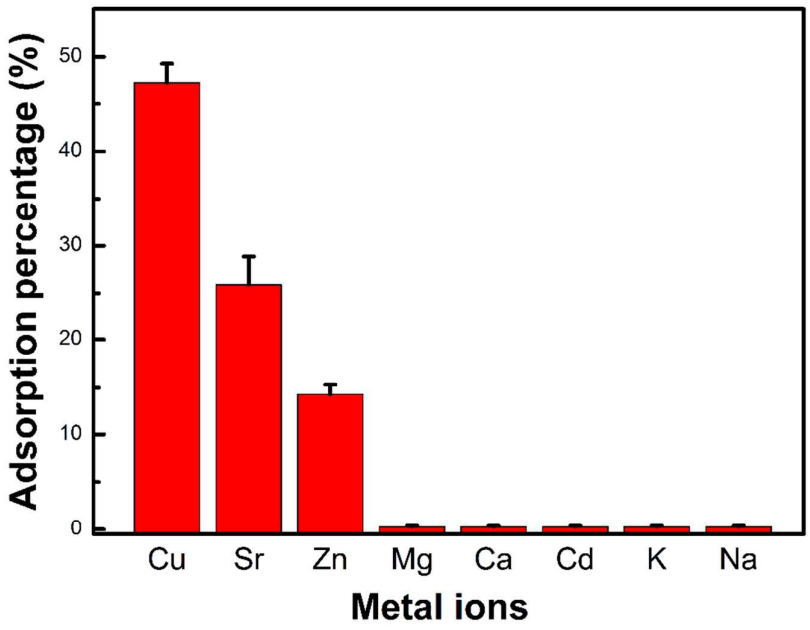

Fig. 11 The competitive adsorption of multi-metal ions, C[metal ions]$_{initial}$=0.8 mmol/L, pH=5, *T*=298 K.

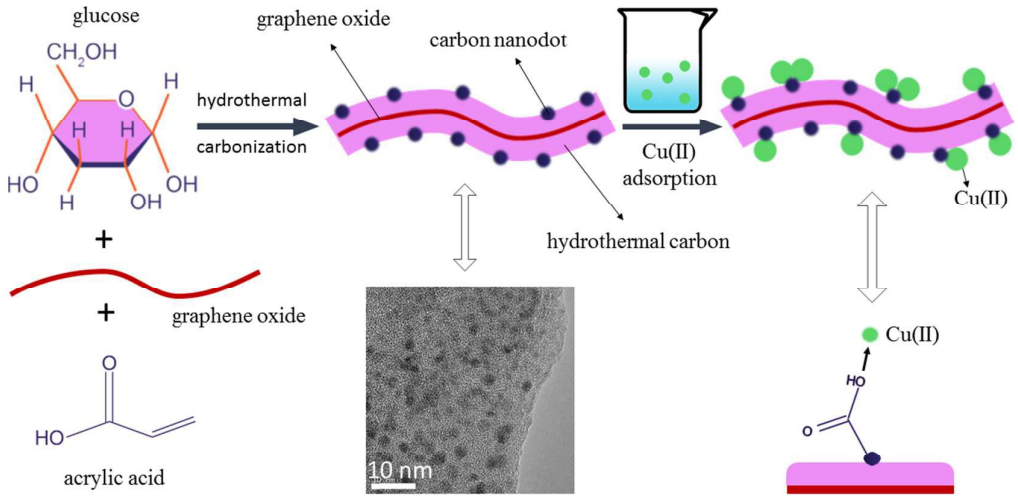

Fig. 12 A schematic diagram elucidating the whole process. The materials were synthesized via one-pot hydrothermal carbonization. Then the materials were used to efficiently remove Cu(II) from aqueous solution.